Steady-State and Transient Analysis of a Steam-Reformer Based Solid Oxide Fuel Cell System

Tuhin Das[1]
Assistant Professor
Department of Mechanical Engineering,
Rochester Institute of Technology,
Rochester, NY 14623
e-mail: tkdeme@rit.edu

Sridharan Narayanan

Ranjan Mukherjee
Professor

Department of Mechanical Engineering,
Michigan State University,
East Lansing, MI 48824

In this paper we perform a model-based analysis of a solid oxide fuel cell (SOFC) system with an integrated steam reformer and with methane as a fuel. The objective of this study is to analyze the steady-state and transient characteristics of this system. For the analysis, we develop a detailed control-oriented model of the system that captures the heat and mass transfer, chemical kinetics, and electrochemical phenomena. We express the dynamics of the reformer and the fuel cell in state-space form. By applying coordinate transformations to the state-space model, we derive analytical expressions of steady-state conditions and transient behaviors of two critical performance variables, namely, fuel utilization and steam-to-carbon balance. Using these results, we solve a constrained steady-state fuel optimization problem using linear programming. Our analysis is supported by simulations. The results presented in this paper can be applied in predicting steady-state conditions and certain transient behaviors and will be useful in control development for SOFC systems. [DOI: 10.1115/1.3120269]

1 Introduction

Among different fuel cell technologies, solid oxide fuel cell (SOFC) systems have generated considerable interest in recent years. Fuel flexibility and tolerance to impurities are attractive attributes of the SOFC systems. Their high operating temperatures (800–1000°C) are conducive to internal reforming of fuel. The exhaust gases are excellent means for sustaining on-board fuel reforming processes. SOFC systems are not only tolerant to carbon monoxide but can also be used as a fuel. They also serve as excellent combined heat and power (CHP) systems. However, the high operating temperatures have precluded automotive applications of the SOFC systems due to the associated thermal stresses, material failure, and significant start-up times.

In this paper we perform a model-based analysis of a steam-reformer based SOFC system with anode recirculation and methane as a fuel. Two types of SOFCs have typically been considered in literature, namely, the planar and the tubular configurations. Mathematical models of the planar version appear in Refs. [1–4], and those of the tubular type appear in Refs. [5–10]. We develop a lumped control-oriented model of a tubular SOFC system. The model serves as a useful simulation tool in the absence of a SOFC hardware. It enables risk-free experimentation and forms the basis of the analytical development presented in this paper. The predominant physical phenomena taking place in the SOFC system, such as heat and mass transfer, chemical kinetics, and electrochemistry, are modeled in detail. The chemical kinetics of steam reforming are modeled based on experimental results and observations presented in Refs. [11,12]. Our model has similarities with the ones presented in Refs. [6,9].

The transient response of a fuel cell system directly impacts its load following capability. Hence, characterization of the transients will be helpful in control design for the cumulative system. One of the earlier works on the transient analysis of the SOFC systems appears in Ref. [13], where the author applied dimensional analysis to characterize voltage transients due to load changes. Transient simulations of a SOFC-gas turbine hybrid system with anode recirculation are presented in Ref. [14]. In Ref. [15], the authors simulate voltage response of a stand-alone SOFC plant to step changes in load and fuel. In Ref. [16], the authors study the detrimental effects of load transients due to differences in the response times of the SOFC, power electronics, and balance-of-plant components. To mitigate these effects, they further investigate the effectiveness of energy buffering devices such as battery.

In this paper we specifically derive analytical expressions that characterize the transient and steady-state behaviors of fuel utilization (U) and steam-to-carbon balance (STCB) of a SOFC system. To the best of our knowledge, such results have not appeared in literature. Utilization is a critical variable in a SOFC system that indicates the ratio of hydrogen consumption to the net available hydrogen in the anode. While high utilization implies high efficiency, very high utilization leads to reduced partial pressure of hydrogen in the fuel cell anode, which can cause irreversible damages due to anode oxidation [9]. Typically, 85% is the target utilization for SOFC systems. Steam-to-carbon ratio (STCR) is another critical variable in steam-reformer based SOFC systems. STCR indicates the availability of steam for fuel reforming at the inlet of the reformer. A minimum STCR, which allows stoichiometric combination of steam and carbon, is necessary. For steam reforming of methane, a stoichiometric mixture has a STCR value of approximately 2. A mixture deficient in steam causes catalyst deactivation through carbon deposition on the catalyst surfaces [14], and therefore must be prevented. In this paper, instead of STCR, we analyze the transient response of the STCB due to its preferred mathematical form. This is justified since a positive STCB automatically implies a mixture with excess steam and hence results in a favorable value of STCR. Both U and STCR/STCB experience dramatic transients due to step changes in load, and our study focuses on predicting these behaviors. These transients arise from the mass transfer and chemical kinetics phenomena. Temperature variation in SOFC systems occurs at a significantly slower rate, and simulations indicate that a quasisteady thermal behavior can be assumed with minimal loss of accuracy.

[1]Corresponding author.

Manuscript received December 22, 2007; final manuscript received August 5, 2008; published online November 11, 2009. Review conducted by Ken Reifsnider. Paper presented at the 2007 ASME International Mechanical Engineering Congress (IMECE2007), Seattle, WA, November 10–16, 2007.

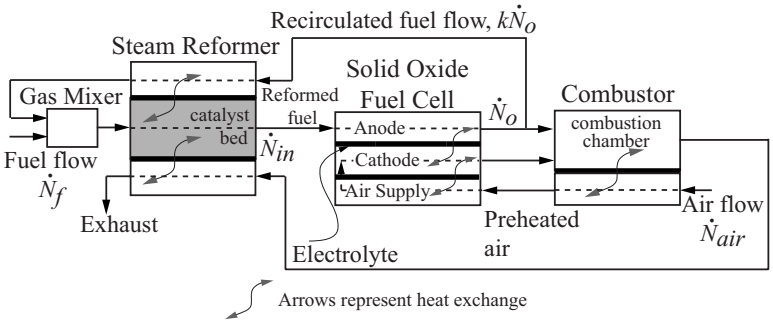

Fig. 1 Schematic of the SOFC system

This paper is organized as follows: In Sec. 2, we first describe the SOFC system under consideration. We then develop the mathematical model of the SOFC system in three subsections. We first present the equations for fundamental gas and solid control volumes. In Secs. 2.1–2.3 we elaborate on the steam reformer and SOFC system models, respectively, with emphasis on the mass transfer phenomena and chemical kinetics. Two open-loop simulations of the system model are provided next for validation against published results and depiction of system trajectories. Steady-state analysis and transient characterization of utilization U and STCR/STCB, due to load changes, are carried out in Secs. 3 and 4, respectively, and simulation results are provided. Based on these results, a steady-state fuel optimization problem is addressed and a minimum fuel operating condition is derived in Sec. 5. Concluding remarks are provided in Sec. 6.

2 SOFC Model Development

2.1 SOFC System Description. Our analysis is based on a steam-reformer based tubular SOFC system. The system consists of three primary components, namely, the steam reformer, which produces a hydrogen-rich gas from a mixture of methane and steam, the solid oxide fuel cell, which generates electricity from electrochemical reactions, and the combustor, where excess fuel is burnt to generate heat. Methane is chosen as the fuel for the system, with a molar flow rate of $\dot{N}_f$. The SOFC system is described in Fig. 1.

The reformer produces a hydrogen-rich gas, which is supplied to the anode of the fuel cell. Electrochemical reactions occurring at the anode due to current draw results in a steam-rich gas mixture at the anode exit. A fraction k of the anode efflux is recirculated through the reformer into a mixing chamber where fuel is added. The mixing of the two fluid streams and pressurization is achieved in the gas mixer using an ejector or a recirculating fuel pump [14,17]. The steam reforming process occurring in the reformer catalyst bed is an endothermic process. The energy required to sustain the process is supplied from two sources, namely, the combustor efflux that is passed through the reformer, and the aforementioned recirculated anode flow, as shown in Fig. 1. The remaining anode efflux is mixed with the cathode efflux in the combustion chamber. The combustor also serves to preheat the cathode air, which has a molar flow rate of $\dot{N}_{\text{air}}$. The tubular construction of each cell causes the air to first enter the cell through the air supply tube and then reverse its direction to enter the cathode chamber. The cathode air serves as the source of oxygen for the fuel cell.

2.2 SOFC System Model

2.2.1 Fundamental Models. The essential dynamics of the SOFC system in Fig. 1 can be represented through fundamental solid volume and gas control volume models.

Solid volume model. The thermodynamics of a solid volume can be expressed as

$$M_s C_s \dot{T}_s = \dot{Q}_s \tag{1}$$

Conductive heat transfers between solid volumes are modeled using Fourier's law of heat conduction. Newton's law of cooling is applied for modeling convective heat transfers between solid and gaseous control volumes [9].

Gas control volume. The gas control volume model consists of energy and mass balance equations and captures the reaction kinetics arising from fuel reforming and electrochemistry. The energy balance equation implemented for the generic gaseous control volume containing a gas mixture is

$$N_g C_v \dot{T}_g = \dot{\eta}_{\text{in}} h_{\text{in}} - \dot{\eta}_{\text{ex}} h_{\text{ex}} + \dot{Q}_g - \dot{W}_{\text{net}} \tag{2}$$

The mass balance equation for individual species is constructed as follows:

$$N_g \dot{\mathcal{X}}_{j,g} = \dot{\eta}_{\text{in}} \mathcal{X}_{j,\text{in}} - \dot{\eta}_{\text{ex}} \mathcal{X}_{j,g} + \mathcal{R}_{j,g}, \quad j = 1,2,\ldots,7 \tag{3}$$

where specific values of subscripts j, $j=1,2,\ldots,7$, correspond to the species CH_4, CO, CO_2, H_2, H_2O, N_2, and O_2, as described in the Nomenclature. From Eq. (3), we additionally have

$$\sum_{j=1}^{7} \mathcal{X}_{j,\text{in}} = \sum_{j=1}^{7} \mathcal{X}_{j,g} = 1 \Rightarrow \sum_{j=1}^{7} \dot{\mathcal{X}}_{j,g} = 0 \Rightarrow \dot{\eta}_{\text{ex}} = \dot{\eta}_{\text{in}} + \sum_{j=1}^{7} \mathcal{R}_{j,g} \tag{4}$$

From Eqs. (2) and (3) it is evident that, in our formulation, the states of the gaseous control volume model are T_g and $\mathcal{X}_{j,g}$, $j=1,2,\ldots,7$. Flow is assumed to be governed by a nominal pressure drop across each module [9], and hence pressure is not treated as a state variable. The gas mixture is assumed to satisfy ideal gas laws and hence N_g in Eqs. (2) and (3) is related to P_g and T_g through the equation $N_g = P_g V_g / R_u T_g$. In Eq. (2), C_v, h_{in}, and h_{ex} are related to the state variables through the following general equations:

$$C_v(T) = \sum_{j=1}^{7} \mathcal{X}_j C_{p,j}(T) - R_u$$

$$C_{p,j}(T)/R_u = a_j + b_j T + c_j T^2 + d_j T^3 + e_j T^4 \tag{5}$$

$$h = h(T) = \sum_{j=1}^{7} \mathcal{X}_j \left(\int_{298}^{T} C_{p,j}(T) dT + \Delta h_{f,j}^{o} \right)$$

where the coefficients a_j, b_j, c_j, d_j, and e_j are given in Ref. [18]. The inlet and exit enthalpies, h_{in} and h_{ex}, are computed as $h_{\text{in}} = h(T_{\text{in}})$ and $h_{\text{ex}} = h(T_{\text{ex}})$.

In Secs. 2.2.2 and 2.2.3, details of the reformer and the fuel cell models are presented. The combustor and gas-mixer models are not required in the analysis presented in Secs. 3–5, and hence omitted for the sake of brevity.

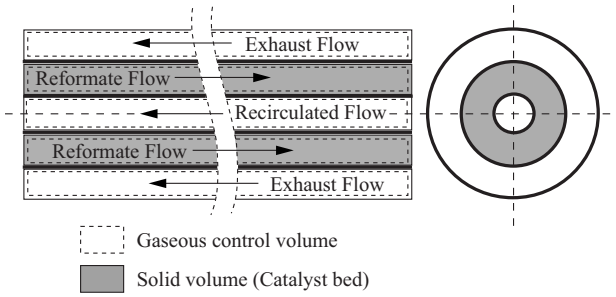

Fig. 2 Schematic of the tubular steam reformer

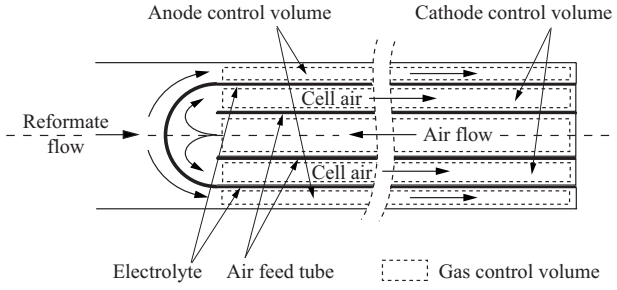

Fig. 3 Schematic of the tubular SOFC

2.2.2 Reformer Model. For steam reforming of methane we consider a packed-bed tubular reformer with nickel-alumina catalyst [19]. A schematic of the steam reformer is shown in Fig. 2.

The exhaust, reformate, and recirculated flows are modeled using gas control volumes, and the catalyst bed is modeled as a solid volume. The details of the heat transfer characteristics of the system can be found in Ref. [9] and are not repeated here. Instead, we emphasize on the reformer reaction kinetics and the mass transfer phenomena in light of the analyses presented in Secs. 3, 4 and 5. The three main reactions that simultaneously occur during steam reforming of methane are [6,12]

$$\begin{aligned} &\text{(I)}\ \ CH_4 + H_2O \leftrightarrow CO + 3H_2 \\ &\text{(II)}\ \ CO + H_2O \leftrightarrow CO_2 + H_2 \\ &\text{(III)}\ \ CH_4 + 2H_2O \leftrightarrow CO_2 + 4H_2 \end{aligned} \tag{6}$$

From Fig. 1, the mass balance equations for CH_4, CO, CO_2, H_2, and H_2O can be written using Eq. (3) as follows:

$$\begin{aligned} N_r\dot{\mathcal{X}}_{1,r} &= k\dot{N}_o\mathcal{X}_{1,a} - \dot{N}_{\text{in}}\mathcal{X}_{1,r} + \mathcal{R}_{1,r} + \dot{N}_f \\ N_r\dot{\mathcal{X}}_{2,r} &= k\dot{N}_o\mathcal{X}_{2,a} - \dot{N}_{\text{in}}\mathcal{X}_{2,r} + \mathcal{R}_{2,r} \\ N_r\dot{\mathcal{X}}_{3,r} &= k\dot{N}_o\mathcal{X}_{3,a} - \dot{N}_{\text{in}}\mathcal{X}_{3,r} + \mathcal{R}_{3,r} \\ N_r\dot{\mathcal{X}}_{4,r} &= k\dot{N}_o\mathcal{X}_{4,a} - \dot{N}_{\text{in}}\mathcal{X}_{4,r} + \mathcal{R}_{4,r} \\ N_r\dot{\mathcal{X}}_{5,r} &= k\dot{N}_o\mathcal{X}_{5,a} - \dot{N}_{\text{in}}\mathcal{X}_{5,r} + \mathcal{R}_{5,r} \end{aligned} \tag{7}$$

where $N_r = P_rV_r/R_uT_r$. Note that the reformer inlet and exit flows shown in Fig. 1 do not contain O_2 and N_2. Hence $\mathcal{X}_{6,r} = \mathcal{X}_{7,r} = 0$. From Eq. (6), we express $\mathcal{R}_{j,r}$, $j = 1, 2, \ldots, 5$, in terms of the reaction rates r_{I}, r_{II}, and r_{III} as follows:

$$\mathbf{R}_r = \mathbf{G}\mathbf{r}, \quad \mathbf{R}_r = \begin{bmatrix} \mathcal{R}_{1,r} \\ \mathcal{R}_{2,r} \\ \mathcal{R}_{3,r} \\ \mathcal{R}_{4,r} \\ \mathcal{R}_{5,r} \end{bmatrix}, \quad \mathbf{r} = \begin{bmatrix} r_{\text{I}} \\ r_{\text{II}} \\ r_{\text{III}} \end{bmatrix}, \quad \mathbf{G} = \begin{bmatrix} -1 & 0 & -1 \\ 1 & -1 & 0 \\ 0 & 1 & 1 \\ 3 & 1 & 4 \\ -1 & -1 & -2 \end{bmatrix} \tag{8}$$

Since $\mathbf{G}$ has a rank of 2, therefore there are only two independent reaction rates among $\mathcal{R}_{j,r}$, $j = 1, 2, \ldots, 5$. Considering the rate of formation of CH_4 and CO in the reformer to be independent, we can write

$$\begin{aligned} \mathcal{R}_{3,r} &= -\mathcal{R}_{1,r} - \mathcal{R}_{2,r} \\ \mathcal{R}_{4,r} &= -4\mathcal{R}_{1,r} - \mathcal{R}_{2,r} \\ \mathcal{R}_{5,r} &= 2\mathcal{R}_{1,r} + \mathcal{R}_{2,r} \end{aligned} \tag{9}$$

and rewrite Eq. (7) as follows:

$$\begin{aligned} N_r\dot{\mathcal{X}}_{1,r} &= k\dot{N}_o\mathcal{X}_{1,a} - \dot{N}_{\text{in}}\mathcal{X}_{1,r} + \mathcal{R}_{1,r} + \dot{N}_f \\ N_r\dot{\mathcal{X}}_{2,r} &= k\dot{N}_o\mathcal{X}_{2,a} - \dot{N}_{\text{in}}\mathcal{X}_{2,r} + \mathcal{R}_{2,r} \\ N_r\dot{\mathcal{X}}_{3,r} &= k\dot{N}_o\mathcal{X}_{3,a} - \dot{N}_{\text{in}}\mathcal{X}_{3,r} - \mathcal{R}_{1,r} - \mathcal{R}_{2,r} \\ N_r\dot{\mathcal{X}}_{4,r} &= k\dot{N}_o\mathcal{X}_{4,a} - \dot{N}_{\text{in}}\mathcal{X}_{4,r} - 4\mathcal{R}_{1,r} - \mathcal{R}_{2,r} \\ N_r\dot{\mathcal{X}}_{5,r} &= k\dot{N}_o\mathcal{X}_{5,a} - \dot{N}_{\text{in}}\mathcal{X}_{5,r} + 2\mathcal{R}_{1,r} + \mathcal{R}_{2,r} \end{aligned} \tag{10}$$

From Eqs. (4) and (10) we deduce

$$\dot{N}_{\text{in}} = k\dot{N}_o + \dot{N}_f + \sum_{j=1}^{7} \mathcal{R}_{j,r} \Rightarrow \dot{N}_{\text{in}} = k\dot{N}_o + \dot{N}_f - 2\mathcal{R}_{1,r} \tag{11}$$

The mathematical functions representing the reaction rates r_{I}, r_{II}, and r_{III} are provided in the Appendix.

2.2.3 SOFC Model. We assume our system to be comprised of $\mathcal{N}_{\text{cell}}$ tubular solid oxide fuel cells, connected in series. A schematic of an individual cell is shown in Fig. 3.

The anode, cathode, and feed air flows are modeled using gas control volumes. The air feed tube and the electrolyte are modeled as solid volumes. Details of the heat transfer model and voltage computations can be found in Ref. [9] and is not repeated here. As in Sec. 2.2.2, we emphasize on the fuel cell chemical kinetics and mass transfer phenomena.

Anode control volume: The following chemical and electrochemical reactions occur simultaneously in the anode control volume:

$$\begin{aligned} &\text{(I)}\ \ CH_4 + H_2O \leftrightarrow CO + 3H_2 \\ &\text{(II)}\ \ CO + H_2O \leftrightarrow CO_2 + H_2 \\ &\text{(III)}\ \ CH_4 + 2H_2O \leftrightarrow CO_2 + 4H_2 \\ &\text{(IV)}\ \ H_2 + O^{2-} \rightarrow H_2O + 2e \end{aligned} \tag{12}$$

Steam reforming, represented by reactions I–III, occur in the anode due to high temperatures and the presence of nickel catalyst. The primary electrochemical process is steam generation from H_2, described by reaction IV. Simultaneous electrochemical conversion of CO to CO_2 in the anode is also possible. However, this electrochemical reaction is ignored since its reaction rate is much slower in the presence of reactions II and IV, as indicated in Ref. [20] and references therein.

From Fig. 1 and Eq. (3), the mass balance equations for CH_4, CO, CO_2, H_2, and H_2O can be written as

$$N_a\dot{\mathcal{X}}_{1,a} = -\dot{N}_o\mathcal{X}_{1,a} + \dot{N}_{\text{in}}\mathcal{X}_{1,r} + \mathcal{R}_{1,a}$$

$$N_a\dot{\mathcal{X}}_{2,a} = -\dot{N}_o\mathcal{X}_{2,a} + \dot{N}_{\text{in}}\mathcal{X}_{2,r} + \mathcal{R}_{2,a}$$

$$N_a\dot{\mathcal{X}}_{3,a} = -\dot{N}_o\mathcal{X}_{3,a} + \dot{N}_{\text{in}}\mathcal{X}_{3,r} + \mathcal{R}_{3,a} \tag{13}$$

$$N_a\dot{\mathcal{X}}_{4,a} = -\dot{N}_o\mathcal{X}_{4,a} + \dot{N}_{\text{in}}\mathcal{X}_{4,r} + \mathcal{R}_{4,a} - r_e$$

$$N_a\dot{\mathcal{X}}_{5,a} = -\dot{N}_o\mathcal{X}_{5,a} + \dot{N}_{\text{in}}\mathcal{X}_{5,r} + \mathcal{R}_{5,a} + r_e$$

where $N_a = P_aV_a/R_uT_a$ and r_e is the rate of electrochemical reaction given by

$$r_e = \frac{i\mathcal{N}_{\text{cell}}}{nF} \tag{14}$$

Since current i can be measured, the rate of electrochemical reaction r_e is considered known. As with the reformate control volume, the anode inlet and exit flows do not contain O_2 and N_2. Therefore, $\mathcal{X}_{6,a} = \mathcal{X}_{7,a} = 0$. From Eq. (12), we express $\mathcal{R}_{j,a}$, $j = 1,2,\ldots,5$, in terms of the reaction rates r_{I}, r_{II}, and r_{III} as follows:

$$\mathbf{R}_a = \mathbf{G}\mathbf{r} + r_e[0 \quad 0 \quad 0 \quad -1 \quad 1]^T \tag{15}$$

where $\mathbf{R}_a = [\mathcal{R}_{1,a}\mathcal{R}_{2,a}\mathcal{R}_{3,a}\mathcal{R}_{4,a}\mathcal{R}_{5,a}]^T$, and $\mathbf{G}$ and $\mathbf{r}$ are given in Eq. (8). Since $\mathbf{G}$ has a rank of 2 and r_e is known, therefore there are only two independent reaction rates among $\mathcal{R}_{j,a}$, $j = 1,2,\ldots,5$. Considering $\mathcal{R}_{1,a}$ and $\mathcal{R}_{2,a}$ to be independent, we can write

$$\mathcal{R}_{3,a} = -\mathcal{R}_{1,a} - \mathcal{R}_{2,a}$$

$$\mathcal{R}_{4,a} = -4\mathcal{R}_{1,a} - \mathcal{R}_{2,a} - r_e \tag{16}$$

$$\mathcal{R}_{5,a} = 2\mathcal{R}_{1,a} + \mathcal{R}_{2,a} + r_e$$

and rewrite Eq. (13) as

$$N_a\dot{\mathcal{X}}_{1,a} = -\dot{N}_o\mathcal{X}_{1,a} + \dot{N}_{\text{in}}\mathcal{X}_{1,r} + \mathcal{R}_{1,a}$$

$$N_a\dot{\mathcal{X}}_{2,a} = -\dot{N}_o\mathcal{X}_{2,a} + \dot{N}_{\text{in}}\mathcal{X}_{2,r} + \mathcal{R}_{2,a}$$

$$N_a\dot{\mathcal{X}}_{3,a} = -\dot{N}_o\mathcal{X}_{3,a} + \dot{N}_{\text{in}}\mathcal{X}_{3,r} - \mathcal{R}_{1,a} - \mathcal{R}_{2,a} \tag{17}$$

$$N_a\dot{\mathcal{X}}_{4,a} = -\dot{N}_o\mathcal{X}_{4,a} + \dot{N}_{\text{in}}\mathcal{X}_{4,r} - 4\mathcal{R}_{1,a} - \mathcal{R}_{2,a} - r_e$$

$$N_a\dot{\mathcal{X}}_{5,a} = -\dot{N}_o\mathcal{X}_{5,a} + \dot{N}_{\text{in}}\mathcal{X}_{5,r} + 2\mathcal{R}_{1,a} + \mathcal{R}_{2,a} + r_e$$

From Eqs. (4) and (17) we deduce that

$$\dot{N}_o = \dot{N}_{\text{in}} + \sum_{j=1}^{7}\mathcal{R}_{j,a} \Rightarrow \dot{N}_o = \dot{N}_{\text{in}} - 2\mathcal{R}_{1,a} \tag{18}$$

The models of internal reforming reaction rates r_{I}, r_{II}, and r_{III} are shown in the Appendix.

Cathode control volume: Ionization of O_2 in the cathode control volume occurs through the reaction

$$0.5O_2 + 2e \rightarrow O^{2-} \tag{19}$$

with the reaction rate as given in Eq. (14). Considering the mole fractions of N_2 and O_2 in air to be 0.79 and 0.21, respectively, the mass balance equations of the cathode control volume can be written from Eqs. (14) and (19) as follows:

$$N_c\dot{\mathcal{X}}_{6,c} = 0.79\dot{N}_{\text{air}} - (\dot{N}_{\text{air}} - 0.5r_e)\mathcal{X}_{6,c}$$

$$N_c\dot{\mathcal{X}}_{7,c} = 0.21\dot{N}_{\text{air}} - (\dot{N}_{\text{air}} - 0.5r_e)\mathcal{X}_{7,c} - 0.5r_e \tag{20}$$

$$\mathcal{X}_{j,c} = 0, \quad j = 1,2,\ldots,5$$

Cell voltage. The cell voltage, V_{cell}, is modeled by subtracting the activation, concentration, and Ohmic losses from the Nernst potential.

$$V_{\text{cell}} = E_{\text{Nernst}} - \Delta V_{\text{act}} - \Delta V_{\text{conc}} - \Delta V_{\text{ohm}} \tag{21}$$

with

$$E_{\text{Nernst}} = E^o + \frac{R_uT}{nF}\ln(\mathcal{X}_{4,a}\mathcal{X}_{7,c}^{0.5}P_c^{0.5}/\mathcal{X}_{5,a})$$

$$\Delta V_{\text{act}} = \frac{R_uT}{\alpha nF}\ln(i/A_{\text{cell}}i_o), \quad \Delta V_{\text{conc}} = -\frac{R_uT}{nF}\ln(1 - i/A_{\text{cell}}i_L), \quad \Delta V_{\text{ohm}} = iR_{\text{eff}}/A_{\text{cell}} \tag{22}$$

where P_c is expressed in the units of atmospheres. Typical values of α, i_o, i_L, and R_{eff} for tubular SOFC are obtained from Refs. [9,21,22].

2.3 Simulations and Model Validation. In this section we provide results of open-loop simulation of the tubular SOFC system model. As experimental data are not available for comparison, we validate our model using published results. We compare the model against the results presented in Refs. [6,9]. Both Refs. [6,9] present data for similar SOFC systems. Specifically, they consider the Siemens Westinghouse tubular SOFC systems [23]. The physical dimensions of each cell are obtained from Refs. [9,23,24]. For this simulation, each cell is assumed to be 50 cm in length and 251 cm^2 in area. The number of cells is chosen as $\mathcal{N}_{\text{cell}} = 576$. The cells are in a series-parallel connection with 3 parallel rows and 192 cells connected in series in each row. The same configuration is used in Ref. [9]. Note that our fuel cell model is sufficiently parametrized, enabling us to predict the impact of parameter variations on the system performance. The above mentioned parameters were chosen to match with published data, for model validation. For the purpose of comparing nominal operating conditions, we set the current demand at 159 A, which is same as that in Ref. [9]. Both Refs. [6,9] use ≈85% as the nominal fuel utilization (U). U is defined as the ratio of H_2 consumption to the net availability of H_2 in the anode volume. We set the fuel (methane) flow to 0.0428 moles/s, which yields $U = 84.6\%$. We set the air flow rate at 30 times the fuel flow rate, which leads to an air utilization ($=0.5r_e/0.21\dot{N}_{\text{air}}$) of ≈29.3%. The anode recirculation is set to 55%, which is close to the nominal value of 54% used in Ref. [6]. We construct two-element discretized models for both the steam reformer and the fuel cell to avoid excessive computational burden while capturing the essential details of the system with sufficient accuracy. Doing this will be helpful in real-time simulation and control development, which is a future goal of this research. A 1500 s simulation of the system in MATLAB®/SIMULINK® took ≈85.7 s on a computer with 2 GHz processor and 4 Gbyte RAM. The simulation yielded the nominal operating condition listed in Table 1.

A comparison of this nominal operating point with those reported in Refs. [6,9] are discussed next. The data of all the variables listed in Table 1 are not reported in Ref. [9]. The cell temperature, stack voltage, and stack power reported in Ref. [9] are 1319.3 K, 128.8 V, and 20.64 kW, respectively, which match closely with the corresponding values in Table 1. The results in Table 1 are compared with those in Ref. [6] (Table 6). The system simulated in Ref. [6] can be considered as a scaled-up version of

Table 1 A nominal operating point obtained through simulation

Variable	Value
No. of cells in series	192
No. of parallel rows	3
Current	159 A
Fuel (methane) flow rate	0.685 g/s
Cell temperature	1300 K
Cell voltage	0.66 V
Stack voltage	126.72 V
Stack power	20.15 kW
Air flow rate	38.5 g/s
Fuel utilization	84.6%
Air utilization	29.3%
Recirculation fraction	0.55
Steam-to-carbon ratio	1.93

our model. The SOFC stack power reported is 191 kW, which is ≈9.5 times the stack power in Table 1. Since the fuel utilization and recirculation fraction used in Ref. [6] are almost same as those in our simulation, we can expect our fuel consumption to be lower by a similar factor. This is indeed the case as 0.685 g/s is ≈10.2 times lower than 7 g/s reported in Ref. [6]. The SOFC temperature and cell voltage reported in Ref. [6] are 1350 K and 0.657 V, respectively, which match closely with those in Table 1. In Ref. [6], the authors report a steam-to-methane ratio of 2. Our simulation yields a STCR of 1.93. The minor difference is due to our definition of STCR, which accounts for the CO in the recirculated flow, in addition to CH_4 in the fuel stream. The exact mathematical definition of STCR used in this paper is given in Sec. 4. The air flow rate reported in Ref. [6] is 445 g/s, which is ≈11.6 times that in Table 1. This leads to approximately 6% difference in the air utilization between our simulation and the corresponding value reported in Ref. [6] (23%). This is attributed to the slight differences in the operating conditions such as fuel utilization and recirculation fraction, and the differences in the electrical and thermal properties of the system considered in the two models.

We next show the results of an open-loop simulation with varying current demands, to illustrate the transient behavior of the system. We arbitrarily consider a system with 100 cells in series, a fuel (pure CH_4) flow of 0.0035 moles/s, air flow of 0.035 moles/s, and a recirculation of 70%. The simulation results are shown in Fig. 4. The load current is changed in steps as shown in Fig. 4(*a*). The cell voltage and temperature changes corresponding to the changes in the current are shown in Figs. 4(*b*) and 4(*d*). Figures 4(*e*) and 4(*f*) depict the molar fractions of the species at reformer exit and anode exit, respectively. The H_2O concentration is higher and the H_2 concentration is lower at the anode exit in comparison to the reformer exit. This is an expected outcome of the current draw. The near equilibrium condition of the water-gas-shift reaction in the anode (reaction II of Eq. (12)) is evident through the sharp depletion of CO corresponding to the depletion of H_2 due to current draw, as shown in Fig. 4(*f*), especially around 500–700 s when the current demand was maximum. Internal reforming in the anode control volume is illustrated by the negligible concentration of CH_4 at the anode exit in Fig. 4(*f*).

In Fig. 4(*c*), utilization U and STCR are plotted. During the interval $0 \le t \le 200$ s, $U \approx 50\%$ and STCR < 1.7. These values imply a low efficiency operation and a mixture marginally deficient in steam at the reformer inlet. This is an undesirable operating condition and is due to excess fuel flow (0.0035 moles/s) with respect to the current demand of 20 A. In contrast, during 550 s $\le t \le 650$ s, $U \approx 85\%$ and STCR ≈ 3.6. This is a favorable operating condition with high efficiency and excess steam at the reformer inlet and is attributed to a higher current draw of 25 A for the same fuel flow.

The SOFC system model presented in Sec. 2 provides a useful platform for model-based analytical studies. The model is comprehensive and captures the primary physical phenomena relevant to the performance of the reformer based SOFC system under consideration. System equations extracted from this model will be used in Secs. 3–5 for further development.

3 Characterization of Utilization

3.1 Steady-State Analysis. Based on the state variable definitions in Eqs. (10) and (17), fuel utilization can be expressed as follows:

$$U = 1 - \frac{\dot{N}_o(4\mathcal{X}_{1,a} + \mathcal{X}_{2,a} + \mathcal{X}_{4,a})}{\dot{N}_{\text{in}}(4\mathcal{X}_{1,r} + \mathcal{X}_{2,r} + \mathcal{X}_{4,r})} \tag{23}$$

Equation (23) is based on the internal reforming capability of the anode where a CH_4 and a CO molecule can yield four molecules and one molecule of H_2, respectively, as indicated by reactions

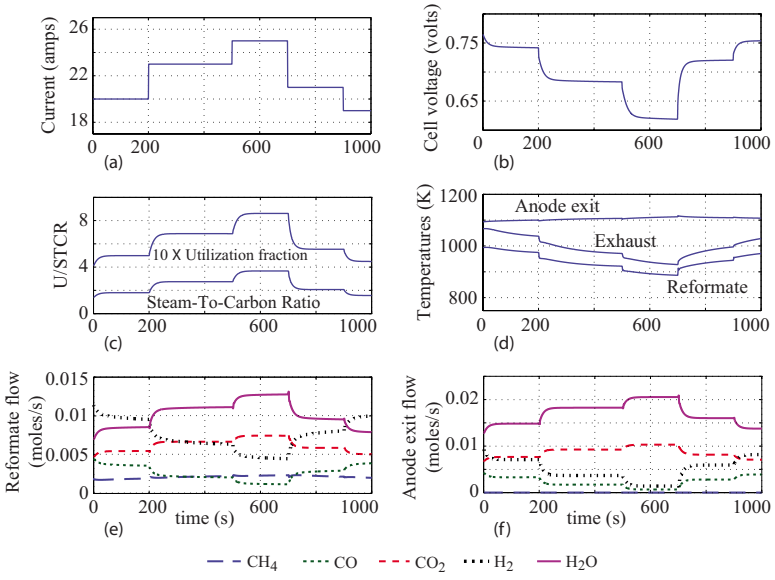

Fig. 4 Open-loop simulation of the fuel cell system

I–III in Eq. (12). We rewrite Eq. (23) with the following coordinate transformations:

$$U = 1 - \frac{\dot{N}_o \zeta_a}{\dot{N}_{\text{in}} \zeta_r}, \quad \begin{matrix} \zeta_r = 4\mathcal{X}_{1,r} + \mathcal{X}_{2,r} + \mathcal{X}_{4,r} \\ \zeta_a = 4\mathcal{X}_{1,a} + \mathcal{X}_{2,a} + \mathcal{X}_{4,a} \end{matrix} \tag{24}$$

Using Eqs. (24), (10), and (17), ζ_r and ζ_a are expressed in the following state-space form:

$$\dot{\mathbf{Z}} = \mathbf{A}_1 \mathbf{Z} + \mathbf{B}_1, \quad \mathbf{Z} = \begin{bmatrix} \zeta_r \\ \zeta_a \end{bmatrix}, \quad \mathbf{A}_1 = \begin{bmatrix} -\dot{N}_{\text{in}}/N_r & k\dot{N}_o/N_r \\ \dot{N}_{\text{in}}/N_a & -\dot{N}_o/N_a \end{bmatrix}, \quad \mathbf{B}_1 = \begin{bmatrix} 4\dot{N}_f/N_r \\ -i\mathcal{N}_{\text{cell}}/nFN_a \end{bmatrix} \tag{25}$$

It is interesting to note here that Eq. (25) is devoid of the reaction rates $\mathcal{R}_{1,r}$, $\mathcal{R}_{2,r}$, $\mathcal{R}_{1,a}$, and $\mathcal{R}_{2,a}$. This is advantageous, but Eq. (25) is nonetheless nonlinear since $\dot{N}_{\text{in}}$, $\dot{N}_o$, N_r, and N_a are nonlinear functions of mole fractions, temperatures, and pressures as follows:

$$\dot{N}_{\text{in}} = \frac{\dot{M}_{\text{in}}}{\sum_{i=1}^{5} \mathcal{X}_{i,r} \text{MW}_i}, \quad \dot{N}_o = \frac{\dot{M}_o}{\sum_{i=1}^{5} \mathcal{X}_{i,a} \text{MW}_i}, \quad N_r = \frac{P_r V_r}{R_u T_r}, \quad N_a = \frac{P_a V_a}{R_u T_a} \tag{26}$$

Since $\mathbf{Z}_{\text{ss}} = \mathbf{A}_1^{-1}\mathbf{B}_1$, from Eqs. (24) and (25) we obtain the following expression for steady-state utilization:

$$U_{\text{ss}} = \frac{1-k}{(4nF\dot{N}_f/i\mathcal{N}_{\text{cell}}) - k} \tag{27}$$

Note that Eq. (27) is independent of the variables in Eq. (26). Furthermore, since k, i, and $\dot{N}_f$ are measurable and known inputs, Eq. (27) can be used to exactly predict the steady-state fuel utilization for any given set of inputs.

3.2 Transient Characteristics. From the definition of U in Eq. (24) note that the transient behavior of U can be predicted from the transient response of ζ_r, ζ_a, $\dot{N}_o$, and $\dot{N}_{\text{in}}$. We specifically consider the transients due to step changes in i, when k and $\dot{N}_f$ are constant. For normal operations, simulations suggest that quasi-static thermal behavior can be assumed, and therefore N_r and N_a can be treated as constants. Also, based on extensive simulations, we make the assumption that, for step changes in i, the variables $\dot{N}_{\text{in}}$ and $\dot{N}_o$ can be treated as constants without significant loss of accuracy. Simulations presented next will confirm the validity of this assumption. With this assumption, Eq. (25) reduces to a linear-time-invariant (LTI) system with eigenvalues of $\mathbf{A}_1$ as

$$\begin{aligned} \lambda_{1,2} &= 0.5[-(\dot{N}_{\text{in}}/N_r + \dot{N}_o/N_a) \pm (|\dot{N}_{\text{in}}/N_r - \dot{N}_o/N_a| + \alpha)] \\ \alpha &= [(\dot{N}_{\text{in}}/N_r - \dot{N}_o/N_a)^2 + 4k(\dot{N}_{\text{in}}/N_r)(\dot{N}_o/N_a)]^{1/2} - |\dot{N}_{\text{in}}/N_r - \dot{N}_o/N_a|, \quad \alpha \geq 0 \end{aligned} \tag{28}$$

Since $k \in (0,1)$, from Eq. (28) it can be verified that the eigenvalues of $\mathbf{A}_1$ are real and negative. The time constant for ζ_r, ζ_a, and U due to a step change in i will be determined by the maximum eigenvalue of $\mathbf{A}_1$. From Eq. (28), we can show that

$$\begin{aligned} &\text{if} \quad \dot{N}_{\text{in}}/N_r \geq \dot{N}_o/N_a \Rightarrow \lambda_{\max} = -\dot{N}_o/N_a + 0.5\alpha \\ &\text{if} \quad \dot{N}_{\text{in}}/N_r < \dot{N}_o/N_a \Rightarrow \lambda_{\max} = -\dot{N}_{\text{in}}/N_r + 0.5\alpha \end{aligned} \tag{29}$$

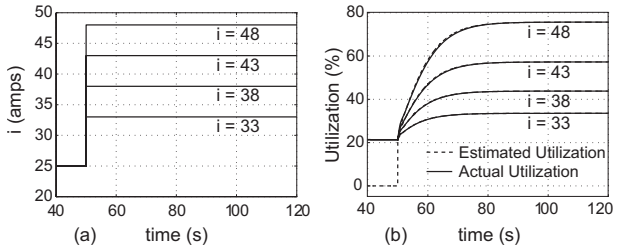

Fig. 5 Transient fuel utilization due to step change in current

We provide simulation results in support of the analysis presented above. We run multiple simulations of the SOFC system with step changes in current applied at $t=50$ s, as shown in Fig. 5.

The steps are from 25 A to 33 A, 38 A, 43 A, and 48 A, as shown in Fig. 5(*a*). In all four simulations, the following settings were used:

$$\dot{N}_f = 0.007 \text{ moles/s}, \quad \dot{N}_{\text{air}} = 0.07 \text{ moles/s}, \quad k = 70\%$$

In Fig. 5(*b*) the transient response of utilization is plotted for the four simulations. It is worthwhile to note that in the plant model, 1D discretized versions of SOFC and reformer models were used. Both units were modeled with two finite elements. In contrast, the estimated utilization are obtained by simulating the lumped model in Eqs. (24) and (25) as a simplified LTI system with $\mathbf{A}_1$ evaluated at the instant $t=50$ s. The following values were observed at $t=50$ s:

$$\begin{matrix} \dot{N}_{\text{in}} = 0.0624 \text{ moles/s} \\ \dot{N}_o = 0.0681 \text{ moles/s} \\ N_r = 0.0263 \text{ mole} \\ N_a = 0.1105 \text{ mole} \end{matrix} \Rightarrow \begin{matrix} \lambda_1 = -2.8347 \\ \lambda_2 = -0.1543 \end{matrix}$$

Both the transient response as well as the steady-state value of estimated utilization match very closely with the nonlinear model-based calculation, as shown in Fig. 5(*b*). The settling time computed based on 2% error is $4/|\lambda_2| = 25.9235$ s, which matches well with the plant model. The accuracy of estimation confirms the validity of our assumption that in predicting transient response, the variables $\dot{N}_{\text{in}}$ and $\dot{N}_o$ can be treated as constants. This is a critical observation that can potentially be applied for control development and for estimation of $\dot{N}_{\text{in}}$ and $\dot{N}_o$ from the transient response of the system using the eigenvalue expressions derived above.

For step changes in $\dot{N}_f$, with i and k held constant, such a linear predictive model cannot be derived. This is due to the direct dependence of $\dot{N}_{\text{in}}$ and $\dot{N}_o$ on $\dot{N}_f$, apparent from Eqs. (11) and (18). This is illustrated in the following sample simulation. Figure 6(*a*) shows the step changes applied to fuel flow in an open-loop simulation. The resulting variations in $\dot{N}_{\text{in}}$ and $\dot{N}_o$ are depicted in Figs. 6(*b*) and 6(*c*), respectively. The variations in these variables are significant and therefore $\dot{N}_{\text{in}}$ and $\dot{N}_o$ cannot be treated as constants during step changes in fuel flow. Thus, a linear system approximation with a constant $\mathbf{A}_1$ matrix, as in Eq. (25), is not possible and an eigenvalue based predictive method cannot be used. Similarly, for step changes in k with $\dot{N}_f$ and i held constant, such a linear predictive model cannot be derived. This is because k is a constituent of the $\mathbf{A}_1$ matrix in Eq. (25). It is worth noting that in tubular fuel cells it may not be possible to actively control k. The anode recirculation is provided by using imperfect seals in tubular SOFC assemblies [23]. The use of imperfect seals not only provides the necessary recirculation but also eliminates the requirement of high-temperature seals.

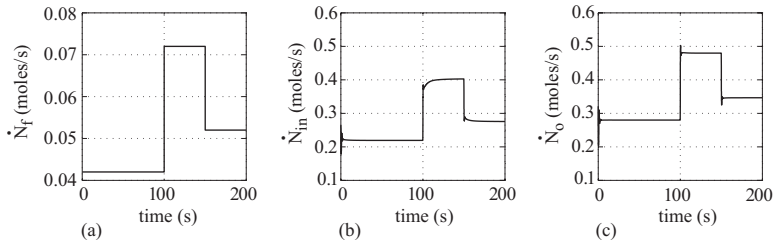

Fig. 6 Response to step changes in fuel flow

4 Characterization of Steam-to-Carbon Balance

4.1 Steady-State Analysis. From Fig. 1, the STCR is expressed as

$$\text{STCR} = \frac{k\dot{N}_o \mathcal{X}_{5,a}}{\dot{N}_f + k\dot{N}_o \mathcal{X}_{1,a} + k\dot{N}_o \mathcal{X}_{2,a}} \tag{30}$$

As indicated by Eq. (30), STCR is the ratio of the concentration of steam molecules to that of carbon atoms at the inlet of the reformer. From reactions II and III of Eq. (6) it is evident that the stoichiometric quantity of steam required for reforming is 2 moles and 1 mole of steam per mole of CH_4 and CO, respectively. With this observation, we define a new variable, namely, the STCB, as follows:

$$\text{STCB} = k\dot{N}_o \mathcal{X}_{5,a} - (2\dot{N}_f + 2k\dot{N}_o \mathcal{X}_{1,a} + k\dot{N}_o \mathcal{X}_{2,a}) = k\dot{N}_o(\mathcal{X}_{5,a} - 2\mathcal{X}_{1,a} - \mathcal{X}_{2,a}) - 2\dot{N}_f \tag{31}$$

A positive value of STCB implies sufficient steam is available at the reformer inlet for reforming and hence a favorable STCR. We rewrite Eq. (31) using the following coordinate transformations:

$$\text{STCB} = k\dot{N}_o \xi_a - 2\dot{N}_f, \quad \begin{matrix} \xi_r = \mathcal{X}_{5,r} - 2\mathcal{X}_{1,r} - \mathcal{X}_{2,r} \\ \xi_a = \mathcal{X}_{5,a} - 2\mathcal{X}_{1,a} - \mathcal{X}_{2,a} \end{matrix} \tag{32}$$

Using Eqs. (32), (10), and (17), the state variable descriptions for ξ_r and ξ_a can be written as

$$\dot{\mathbf{S}} = \mathbf{A}_2\mathbf{S} + \mathbf{B}_2, \quad \mathbf{S} = \begin{bmatrix} \xi_r \\ \xi_a \end{bmatrix}, \quad \mathbf{A}_2 = \begin{bmatrix} -\dot{N}_{\text{in}}/N_r & k\dot{N}_o/N_r \\ \dot{N}_{\text{in}}/N_a & -\dot{N}_o/N_a \end{bmatrix}, \quad \mathbf{B}_2 = \begin{bmatrix} -2\dot{N}_f/N_r \\ i\mathcal{N}_{\text{cell}}/nFN_a \end{bmatrix} \tag{33}$$

Note that the variables ξ_r and ξ_a in Eq. (33) are independent of $\mathcal{R}_{1,r}$, $\mathcal{R}_{2,r}$, $\mathcal{R}_{1,a}$, and $\mathcal{R}_{2,a}$. However, Eq. (33) is nonlinear since $\dot{N}_{\text{in}}$, $\dot{N}_o$, N_r, and N_a are nonlinear functions of the mole fractions, temperatures, and pressures (see Eq. (26)). From Eq. (33), we obtain the following steady-state expression for STCB:

$$\text{STCB}_{\text{ss}} = \frac{1}{k-1}\left(2\dot{N}_f - \frac{ki\mathcal{N}_{\text{cell}}}{nF}\right) \tag{34}$$

4.2 Transient Characteristics. From Eqs. (25) and (33), we note that $\mathbf{A}_2 = \mathbf{A}_1$. Hence, the time constant of STCB due to step input in current can be estimated using the eigenvalues λ_1 and λ_2 of $\mathbf{A}_1$ given in Eq. (28). The simulation results provided here are a continuation of those in Fig. 5 in Sec. 3.2. In Figs. 7(*a*) and 7(*b*), STCR and STCB are plotted for the four simulations described in Fig. 5(*a*). In Fig. 7(*b*) the transient response of STCB is plotted. The estimated STCB is computed by considering the system given in Eqs. (32) and (33) as a LTI system with $\mathbf{A}_2$ evaluated at the instant $t = 50$ s. Both the transient response as well as the steady-state value of estimated STCB match very closely with the model-based calculation, as shown in Fig. 7(*b*). As with U, the transient characteristics of STCB, for step changes in $\dot{N}_f$ and k, cannot be predicted using an approximate lumped linear model since these inputs directly impact the $\mathbf{A}_2$ matrix.

5 Steady-State Fuel Optimization

5.1 Problem Statement. Using the results derived in Secs. 3 and 4, we address a steady-state constrained fuel optimization problem, which is stated as follows: Given that utilization and anode recirculation must be constrained within ranges $U_{\text{ss}} \in [U_{\text{ss1}}, U_{\text{ss2}}]$, $0 < U_{\text{ss1}}, U_{\text{ss2}} < 1$ and $k \in [k_a, k_b]$, $0 < k_a, k_b < 1$, respectively, and given a current i, we did the following.

1. Determine condition(s) under which there exists a range of solutions for $\dot{N}_f$ that satisfies the constraints above and maintains $\text{STCB} \geq 0$.
2. If a range of solutions exists, determine the minimum fuel operating conditions.

5.2 Optimum Fuel Operation. From Eq. (34), note that for ensuring a steam-rich inlet flow into the reformer, we must have

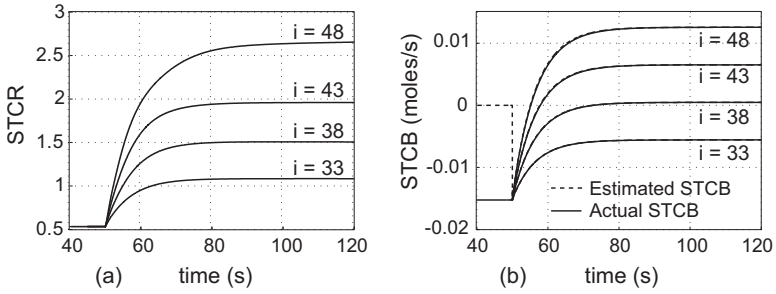

Fig. 7 Transient STCR and STCB due to step change in current

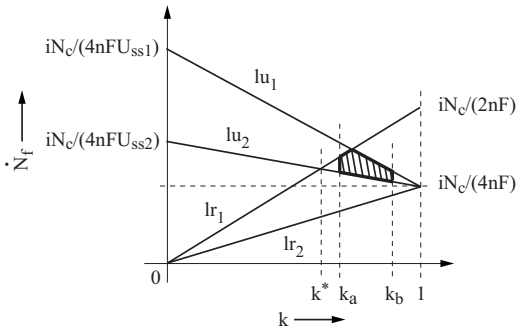

Fig. 8 Steady-state fuel optimization

$$\mathrm{STCB_{ss}} \geq 0 \Rightarrow \dot{N}_f \leq k\left(\frac{i\mathcal{N}_{\mathrm{cell}}}{2nF}\right) \tag{35}$$

From Eq. (27) we have

$$U_{\mathrm{ss}} \geq 0 \Rightarrow \dot{N}_f \geq k\left(\frac{i\mathcal{N}_{\mathrm{cell}}}{4nF}\right) \tag{36}$$

and the constraints $0 < U_{\mathrm{ss1}} \leq U_{\mathrm{ss}} \leq U_{\mathrm{ss2}} < 1$ are expressed as

$$\dot{N}_f\left(\frac{4nFU_{\mathrm{ss1}}}{i\mathcal{N}_{\mathrm{cell}}}\right) + (1 - U_{\mathrm{ss1}})k \leq 1 \tag{37}$$

$$\dot{N}_f\left(\frac{4nFU_{\mathrm{ss2}}}{i\mathcal{N}_{\mathrm{cell}}}\right) + (1 - U_{\mathrm{ss2}})k \geq 1 \tag{38}$$

Equations (35)–(38) are all linear in $\dot{N}_f$ and k and are denoted in Fig. 8 by lr_1, lr_2, lu_1, and lu_2, respectively, along with the lines $k=k_a$ and $k=k_b$. Steady-state constrained fuel optimization for the steam-reformer based SOFC system has thus been transformed into a problem in linear programming. From Fig. 8 and from Eqs. (35)–(38), we can easily deduce that a solution region exists if $k_b \geq k^*$, where k^* is the value of k at the intersection between the lines lr_1 and lu_2. Hence, from Eqs. (35) and (38) we have

$$k^* = \frac{1}{1 + U_{\mathrm{ss2}}} \Rightarrow k_b \geq \frac{1}{1 + U_{\mathrm{ss2}}} \tag{39}$$

From Fig. 8 it is also evident that if Eq. (39) is satisfied, then the steady-state minimum fuel operating point is at the intersection of lu_2 and $k=k_b$, given by

$$k = k_b, \quad U = U_{\mathrm{ss2}}, \quad \dot{N}_{f,\min} = \frac{i\mathcal{N}_{\mathrm{cell}}}{4nFU_{\mathrm{ss2}}}[1 - (1 - U_{\mathrm{ss2}})k_b] \tag{40}$$

5.3 Simulations. Steady-state minimum fuel operation is demonstrated using the following simulation results. We consider a system with 100 cells in series and $i=50$ A. It is desired to attain the steady-state minimum fuel operating point under the constraints, $U_{\mathrm{ss1}}=0.6$, $U_{\mathrm{ss2}}=0.85$, $k_a=0.6$, $k_b=0.8$, and $\mathrm{STCB_{ss}} \geq 0$. We choose the initial operating conditions $k=0.65$ and $\dot{N}_f = 0.01$ moles/s, and set the air flow rate at $\dot{N}_a = 10\dot{N}_f$ for the entire simulation. The simulation results are shown below in Fig. 9. In Fig. 9(*a*), the lines lr_1, lr_2, lu_1, and lu_2, representing Eqs. (35)–(38), are plotted and the trajectory of the operating point in ($\dot{N}_f$ versus k) space is superimposed. The initial condition corresponds to point *A* in Fig. 9(*a*). At this operating point, the model is first simulated in open-loop mode up to $t_1=40$ s. Note that at *A*, the conditions $U_{\mathrm{ss1}} \leq U_{\mathrm{ss}} \leq U_{\mathrm{ss2}}$ and $\mathrm{STCB_{ss}} \geq 0$ are not satisfied. Specifically, at *A*, $U_{\mathrm{ss}} \approx 0.4$ and $\mathrm{STCB_{ss}} \approx -0.01$ moles/s, as shown in Figs. 9(*b*) and 9(*e*), respectively. At t_1, a proportional-integral control is invoked to control utilization by varying $\dot{N}_f$. Simultaneously, the target utilization is ramped from 0.45 at t_1 to 0.85 at $t_3=240$ s, as shown in Fig. 9(*b*). This leads to a reduction in $\dot{N}_f$, depicted in Fig. 9(*c*), from 0.01 moles/s to 6.878×10^{-3} moles/s. During this interval k is maintained at 0.65, as shown in Fig. 9(*d*), and the operating point in Fig. 9(*a*) shifts from point *A* to *B*. Also note from Fig. 9(*e*) that $\mathrm{STCB} > 0$ for $t > t_2$. At $t_4=300$ s, k is ramped from 0.65 to $k_b=0.8$ at $t_5=450$ s. This leads to further reduction in $\dot{N}_f$ to 6.705×10^{-3} moles/s, as shown in Fig. 9(*c*). The corresponding shift in the operating point from *B* to *C* is shown in Fig. 9(*a*). The minimum fuel operating point as computed using Eq. (40) is 6.706×10^{-3} moles/s, which matches very closely with that obtained through simulation. It must be noted that the proportional-integral control implemented here is not a proposed control strategy. It is used to automatically arrive at the minimum fuel operating point and thus it serves to validate Eq. (40).

6 Conclusion

In this paper we have presented an analytical study of steady-state and transient behaviors of a SOFC system due to changes in current demand. For the analysis we considered a steam-reformer based tubular SOFC system with anode recirculation and with methane as fuel. We developed a detailed control-oriented model

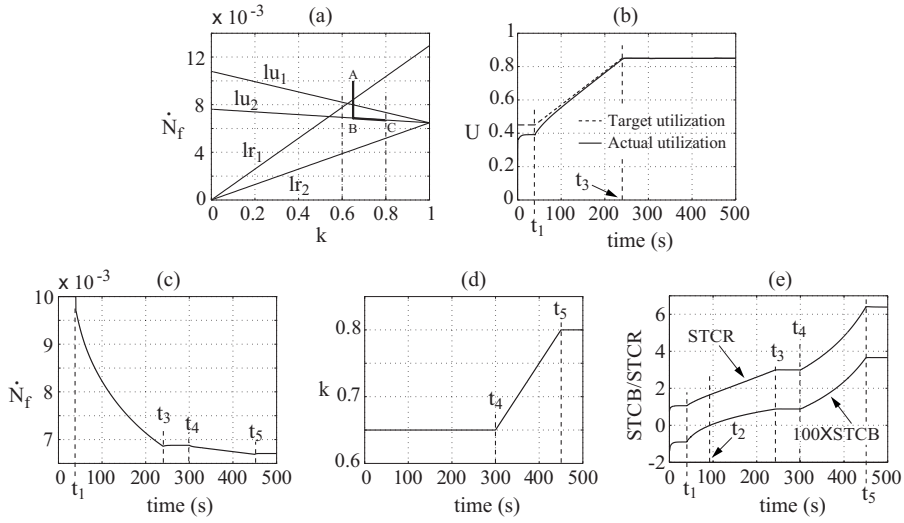

Fig. 9 Fuel optimization simulation

for the SOFC system and expressed the mass transfer and chemical kinetics phenomena of the reformer and anode control volumes in state-space form. Our model was validated against published papers. We derived closed-form expressions that characterizes the steady-state and transient behaviors of fuel utilization (U) and STCB. Our analysis was facilitated by key coordinate transformations that eliminated nonlinear reaction rate terms from the coupled dynamic equations of the reformer and anode volumes. For predicting the transient response to step changes in current, we treated the molar flow rates $\dot{N}_{\text{in}}$ and $\dot{N}_o$ as constants. These steps simplified the nonlinear system to a lumped linear-time-invariant form with minimal loss of accuracy. The estimates of time constants and steady-state values of U and STCB, generated by the simplified model, matched very closely with those generated by the discretized nonlinear plant model. A similar linear system approximation could not be applied for predicting transients due to step changes in $\dot{N}_f$ and k. The steady-state results were applied to address a fuel optimization problem for the SOFC system using the linear-programming approach. The constrained optimization problem yielded a minimum fuel operating point. The analytical results were confirmed through simulations.

Nomenclature

A_{cell} = cell area, m^2
C = specific heat, J/kg K
C_p = specific heat at constant pressure, J/kg K
C_v = specific heat at constant volume, J/kg K
E_{I}, E_{II}, E_{III} = activation energy of reforming reactions I, II, and III, J/mol
E_{Nernst} = Nernst potential, V
F = Faraday's constant, 96,485.34 C/mol
h = molar enthalpy, J/mol
i = current draw, A
i_o, i_L = exchange and limiting current density, A/m^2
k = anode recirculation fraction
M = mass, kg
MW = molecular weight, kg/mol
$\dot{M}_{\text{in}}$ = anode inlet mass flow rate, kg/s
$\dot{M}_o$ = anode exit mass flow rate, kg/s
N = number of moles, moles
$\dot{N}_{\text{air}}$ = molar flow rate of air, moles/s
$\dot{N}_f$ = molar flow rate of fuel, moles/s
$\dot{N}_{\text{in}}$ = anode inlet flow rate, moles/s
$\dot{N}_o$ = anode exit flow rate, moles/s
n = number of electrons participating in the electrochemical reaction, (=2)
P = pressure, Pa
p = partial pressure, Pa
$\dot{Q}$ = net rate of heat transfer into a solid or gaseous volume, W
R_{cell} = internal cell resistance, $\Omega\ \text{m}^2$
R_u = universal gas constant, 8.314 J/mol K
r_{I}, r_{II}, r_{III} = rates of reforming reactions I, II, and III, moles/s
r_e = rate of electrochemical reaction, moles/s
T = temperature, K
T_{ref} = reference temperature, K
U = utilization
V = volume, m^3
$\dot{W}_{\text{net}}$ = net rate of work done, W
α = transfer coefficient
ΔH = enthalpy of reaction or adsorption, J/mol
Δh_f^o = enthalpy of formation at 298 K and 1 atm pressure, J/mol
ΔV_{act}, ΔV_{conc}, ΔV_{ohm} = activation, concentration, and Ohmic overpotentials, V
$\mathcal{K}_{\text{I}}$, $\mathcal{K}_{\text{III}}$ = equilibrium constant of reactions I and III, Pa^2
$\mathcal{K}_{\text{II}}$ = equilibrium constant of reaction II
$\mathcal{K}_{\text{CH}_4}$, $\mathcal{K}_{\text{CO}}$, $\mathcal{K}_{\text{H}_2}$ = adsorption constant for CH_4, CO, H_2, Pa^{-1}
$\mathcal{K}_{\text{H}_2\text{O}}$ = adsorption constant for H_2O
κ_{I}, κ_{III} = rate coefficient of reactions I and III, mol $\text{Pa}^{0.5}$/kg cat. s
κ_{II} = rate coefficient of reaction II, moles/kg cat. s Pa
$\mathcal{N}_{\text{cell}}$ = number of cells
$\dot{\eta}$ = molar flow rate, moles/s
$\mathcal{R}$ = species rate of formation, moles/s
$\mathcal{X}$ = species mole fraction

Subscripts

a = anode control volume
c = cathode control volume
cat = catalyst
ex = exit condition of control volume
g = generic gas control volume
in = inlet condition of control volume
j = values of 1–7 represent the species CH_4 CO, CO_2, H_2, H_2O, N_2, and O_2, respectively
r = reformate control volume
s = solid volume
ss = steady-state

Appendix

We use the following reaction rate expressions, given in Ref. [12], to model the kinetics of steam reforming reactions in Eqs. (6) and (12). The equations below are written for a generic gas control volume. For the SOFC system, these equations apply for the reforming reactions in the reformate control volume as well as the anode control volume.

$$r_{\text{I}} = \frac{M_{\text{cat}}\kappa_{\text{I}}}{p_{\text{H}_2}^{2.5}}\left(p_{\text{CH}_4}p_{\text{H}_2\text{O}} - \frac{p_{\text{H}_2}^3 p_{\text{CO}}}{\mathcal{K}_{\text{I}}}\right)/\delta^2 \tag{A1}$$

$$r_{\text{II}} = \frac{M_{\text{cat}}\kappa_{\text{II}}}{p_{\text{H}_2}}\left(p_{\text{CO}}p_{\text{H}_2\text{O}} - \frac{p_{\text{H}_2}p_{\text{CO}_2}}{\mathcal{K}_{\text{II}}}\right)/\delta^2 \tag{A2}$$

$$r_{\text{III}} = \frac{M_{\text{cat}}\kappa_{\text{III}}}{p_{\text{H}_2}^{3.5}}\left(p_{\text{CH}_4}p_{\text{H}_2\text{O}}^2 - \frac{p_{\text{H}_2}^4 p_{\text{CO}_2}}{\mathcal{K}_{\text{III}}}\right)/\delta^2 \tag{A3}$$

where

$$\delta = 1 + \mathcal{K}_{\text{CO}}p_{\text{CO}} + \mathcal{K}_{\text{H}_2}p_{\text{H}_2} + \mathcal{K}_{\text{CH}_4}p_{\text{CH}_4} + \mathcal{K}_{\text{H}_2\text{O}}p_{\text{H}_2\text{O}}p_{\text{H}_2}$$

$$p_j = \mathcal{X}_j P_g, \quad j = 1,2,\ldots,5 \tag{A4}$$

In Eqs. (A1)–(A3), the rate coefficients κ_{I}, κ_{II}, and κ_{III} are given by

$$\kappa_f = \kappa_{f,T_{\text{ref}}} \exp\left[-\frac{E_f}{R_u}\left(\frac{1}{T_g} - \frac{1}{T_{\text{ref},f}}\right)\right], \quad f = \text{I,II,III} \tag{A5}$$

and the adsorption constants $\mathcal{K}_{\text{CO}}$, $\mathcal{K}_{\text{H}_2}$, $\mathcal{K}_{\text{CH}_4}$, and $\mathcal{K}_{\text{H}_2\text{O}}$ are given as follows:

$$\mathcal{K}_q = \mathcal{K}_{q,T_{\text{ref}}} \exp\left[-\frac{\Delta H_q}{R_u}\left(\frac{1}{T_g} - \frac{1}{T_{\text{ref},q}}\right)\right], \quad q = \text{CO}, \text{H}_2, \text{CH}_4, \text{H}_2\text{O} \tag{A6}$$

where the values of E_f, $T_{\text{ref},f}$, and $\kappa_{f,T_{\text{ref}}}$, with $f=\text{I}, \text{II}, \text{III}$, and ΔH_q, $T_{\text{ref},q}$, and $\mathcal{K}_{q,T_{\text{ref}}}$, with $q=\text{CO}$, H_2, CH_4, and H_2O, are given in Ref. [12].

References

[1] Aguiar, P., Adjiman, C. S., and Brandon, N. P., 2005, "Anode Supported Intermediate-Temperature Direct Internal Reforming Solid Oxide Fuel Cell, II. Model-Based Dynamic Performance and Control," J. Power Sources, **147**, pp. 136–147.

[2] Campanari, S., and Iora, P., 2005, "Comparison of Finite Volume SOFC Models for the Simulation of a Planar Cell Geometry," Fuel Cells, **5**, pp. 34–51.

[3] Lu, N., Li, Q., Sun, X., and Khaleel, M. A., 2006, "The Modeling of a Standalone Solid-Oxide Fuel Cell Auxiliary Power Unit," J. Power Sources, **161**, pp. 938–948.

[4] Xi, H., Sun, J., and Tsourapas, V., 2007, "A Control Oriented Low Order Dynamic Model for Planar SOFC Using Minimum Gibbs Free Energy Method," J. Power Sources, **165**, pp. 253–266.

[5] Hall, D. J., and Colclaser, R. G., 1999, "Transient Modeling and Simulation of a Tubular Solid Oxide Fuel Cell," IEEE Trans. Energy Convers., **14**(3), pp. 749–753.

[6] Kandepu, R., Imsland, L., Foss, B. A., Stiller, C., Thorud, B., and Bolland, O., 2007, "Modeling and Control of a SOFC-GT-Based Autonomous Power System," Energy, **32**, pp. 406–417.

[7] Lazzaretto, A., Toffolo, A., and Zanon, F., 2004, "Parameter Setting for a Tubular SOFC Simulation Model," ASME J. Energy Resour. Technol., **126**, pp. 40–46.

[8] Li, P., and Chyu, M. K., 2003, "Simulation of the Chemical/Electrochemical Reactions and Heat/Mass Transfer for a Tubular SOFC in a Stack," J. Power Sources, **124**, pp. 487–498.

[9] Mueller, F., Brouwer, J., Jabbari, F., and Samuelsen, S., 2006, "Dynamic Simulation of an Integrated Solid Oxide Fuel Cell System Including Current-Based Fuel Flow Control," ASME J. Fuel Cell Sci. Technol., **3**, pp. 144–154.

[10] Xue, X., Tang, J., Sammes, N., and Du, Y., 2005, "Dynamic Modeling of Single Tubular SOFC Combining Heat/Mass Transfer and Electrochemical Reaction Effects," J. Power Sources, **142**, pp. 211–222.

[11] Achenbach, E., and Riensche, E., 1994, "Methane/Steam Reforming Kinetics for Solid Oxide Fuel Cells," J. Power Sources, **52**, pp. 283–288.

[12] Xu, J., and Froment, G. F., 1989, "Methane Steam Reforming, Methanation and Water-Gas Shift: I. Intrinsic Kinetics," AIChE J., **35**(1), pp. 88–96.

[13] Achenbach, E., 1995, "Response of a Solid Oxide Fuel Cell to Load Change," J. Power Sources, **57**, pp. 105–109.

[14] Ferrari, M. L., Traverso, A., Magistri, L., and Massardo, A. F., 2005, "Influence of Anodic Recirculation Transient Behavior on the SOFC Hybrid System Performance," J. Power Sources, **149**, pp. 22–32.

[15] Sedghisigarchi, K., and Feliachi, A., 2004, "Dynamic and Transient Analysis of Power Distribution Systems With Fuel Cells-Part 1: Fuel-Cell Dynamic Model," IEEE Trans. Energy Convers., **19**(2), pp. 423–428.

[16] Mazumder, S. K., Pradhan, S. K., Acharya, K., Hartvigsen, J., von Spakovsky, M. R., and Haynes, C., 2004, "Load Transient Mitigation Techniques for Solid-Oxide Fuel Cell (SOFC) Power-Conditioning System," *INTELEC 2004*, 26th Annual International Telecommunications Energy Conference, pp. 174–181.

[17] Karnik, A. Y., and Sun, J., 2005, "Modeling and Control of an Ejector Based Anode Recirculation System for Fuel Cells," *Proceedings of the ASME Fuel Cell Conference*, ASME, New York, pp. 721–731.

[18] Wark, K., 1988, *Thermodynamics*, 5th ed., McGraw-Hill, New York.

[19] Incropera, F. P., and DeWitt, D. P., 2002, *Fundamentals of Heat and Mass Transfer*, 5th ed., Wiley, New York.

[20] Bove, R., Lunghi, P., and Sammes, N. M., 2005, "SOFC Mathematic Model for Systems Simulations-Part 2: Definition of an Analytical Model," Int. J. Hydrogen Energy, **30**, pp. 189–200.

[21] Li, X., 2006, *Principles of Fuel Cells*, Taylor & Francis, New York.

[22] Roberts, R. A., and Brouwer, J., 2006, "Dynamic Simulation of a Pressurized 220 kW Solid Oxide Fuel Cell-Gas Turbine Hybrid System: Modeled Performance Compared to Measured Results," ASME J. Fuel Cell Sci. Technol., **3**, pp. 18–25.

[23] Larminie, J., and Dicks, A., 2003, *Fuel Cell Systems Explained*, 2nd ed., Wiley, New York.

[24] Roberts, C. A., George, R. A., Veyo, S. E., and Casanova, A. C., 2000, "Demonstrations: The Bridge to Commercialization for the SOFC," Electricity Today Magazine, http://www.electricity-today.com, Jun.